Unveiling Key Limitations of ZnO/Cu 2 O All-Oxide Solar Cells through Numerical Simulations

Abderrahime Sekkat, Daniel Bellet, Guy Chichignoud, David Muñoz-Rojas, Anne Kaminski-Cachopo

Unveiling Key Limitations of ZnO/Cu_2O All-Oxide Solar Cells through Numerical Simulations Approach

Abderrahime Sekkat[1,2,3,], Daniel Bellet[1], Guy Chichignoud[3], David Muñoz-Rojas[1,*], Anne Kaminski-Cachopo[2,*]*

[1] Univ. Grenoble Alpes, CNRS, Grenoble INP, LMGP, F-38000 Grenoble, France

[2] Univ. Grenoble Alpes, Univ. Savoie Mont Blanc, CNRS, Grenoble INP, IMEP-LaHC, 38000 Grenoble, France

[3] Univ. Grenoble Alpes, CNRS, Grenoble INP, SIMAP, 38000 Grenoble, France.

KEYWORDS: ZnO/Cu_2O; numerical simulation; SCAPS-1D; performances; working mechanism

ABSTRACT:

ZnO/Cu_2O solar cells emerge as one of the most promising technologies with significant potential when considering the Schockley-Queisser limit (SQL), and taking into consideration other important factors such as materials abundance, low-cost fabrication, suitable band alignment, and the possibility of having semi-transparent devices. However, the actual efficiency values obtained are still far from the expected theoretical values. The reasons behind this are mainly attributed to the low control over the properties of the oxides and the knowledge on how the final device

performance is affected by both materials properties and cell architecture. To close this gap, we explore the working mechanism of ZnO/Cu_2O junctions thanks to numerical simulations based on the SCAPS-1D software. In particular, the present study aims at investigating the limiting factors and key parameters that affect the behavior of the ZnO/Cu_2O junctions. The impact of altering: the absorber and collector film thickness, the diffusion length, side illumination, and the concentration of defects at the junction interface are explored. The data indicates that the thickness of Cu_2O is critical for the output results when correlated with the diffusion length, which in turn is strongly affected by the oxide deposition technique and conditions. Bifacial illumination demonstrates a significant enhancement of the power conversion efficiency while defects at the interface inhibit the charge generation drastically and enhance recombination at the sub-cell level. This study provides an overarching view of cell behavior and different routes towards the improvement of ZnO/Cu_2O devices.

1. INTRODUCTION

The interest in developing all-oxide solar cells has been growing significantly due to their potential in terms of low-cost and environmentally friendly characteristics. In particular, homojunction Cu_2O solar cells present a theoretical efficiency of 20% according to the Schockley-Queisser limit (SQL)[1,2]. Cu_2O being intrinsically p-type, n-type Cu_2O is very challenging to obtain[3]. Therefore, Cu_2O has been mostly combined with n-type ZnO[4,5]. However, the maximum achieved efficiencies for Cu_2O/ZnO devices are only around ~ 1-2% so far[5–13] (excluding doping or interface engineering). Several factors limit the power conversion efficiency (PCE) of ZnO/Cu_2O solar cells, namely, material and charge collector quality, material absorption

coefficient, and interface quality[14–16]. Thus, efforts must be made towards comprehending the cell behavior and the most significant parameters for achieving optimum performance.

Modeling has been performed on all-oxide solar cells comprising Cu_2O as the main absorber[17–20]. Different structures, i.e. (AZO/ZnGeO/Cu_2O)[21], (ZnO/CuO/Cu_2O)[19], (AZO/ZnO/Defective layer/Cu_2O)[22], have been studied to understand the various mechanisms taking place. However, the main focus is commonly on simulating Cu_2O thin films combined with several layers (i.e. buffer, tandem, and transparent conductive oxides)[17–19,22–25] or on the analysis of optical properties of Cu_2O based solar devices[20,26]. Previous experimental studies have already shown that film thickness, band alignment, and defects (both affected by the deposition method and conditions used) are the main factors affecting cell performance[18,19,22]. One of the main achievements of these results is the improvement of the cell efficiency with different structures through introducing different interfaces and defective layers at the junction interface[17,22,24]. Other studies combining experimental and simulation results have addressed in depth the impact of film defects on the quantum efficiency of cells[6,14]. The latter have shown that the EQE of Cu_2O-based solar cells changes drastically with the type of defects (interfacial or bulk) and interface roughness[6,14]. Various softwares have been used for simulation Cu_2O based solar cells, mainly SCAPS-1D[19,25,27], wxAMPS[17,28,29], and Silvaco TCAD[30]. Although the reports above provide valuable insight on the limitations of ZnO/Cu_2O solar cells, more efforts are needed to guide the optimization of simpler ZnO/Cu_2O devices, i.e. without the introduction of additional layers, towards higher efficiencies than the ones achieved so far.

In the present study, a simple planar ZnO(n)/Cu_2O(p) structure is modeled with the SCAPS-1D software. The solar cell capacitance simulator SCAPS[31] is a simulation software, similar to PC1D[32] or wxAMPS[28], which was developed at the University of Gent (Belgium) at the Department of

Electronics and Information Systems (ELIS). The thicknesses of ZnO and Cu_2O thin films are varied and their influence on the device performance is evaluated. Illumination from either sides or bi-facial illumination is introduced here to evaluate the change in the light collection and charge separation. The influence of the diffusion length value on the Cu_2O thin film is also analyzed. The presence of defects at the junction (which can be affected by the deposition method, post-deposition treatments or cell architecture[33], for example) is introduced, and the resulting recombination is assessed. Our study is thus more complete than previous reports and the results show that both Cu_2O and ZnO thickness are key parameters being affected by the diffusion length of minority charge carriers. We also show that limiting the presence of defects at the interface and bifacial illumination are suitable strategies to maximize the efficiency and potential of these devices.

2. METHODS

The modeling in this work is based on SCAPS software that was provided by Prof. Marc Burgelman (University of Gent)[31]. As a first approach, the strategy is oriented towards implementing experimental data obtained on metal oxides (Cu_2O & ZnO). The refractive index and the extinction coefficient were extracted from C. Malerba *et al.*[34], for Cu_2O, and from C. Stelling *et al.*[35], for ZnO. These parameters were included in a text file that is integrated into the software. Then, the absorption coefficient was calculated based on the Beer-Lambert law and "Eg-sqrt" model, since it is related to the extinction coefficient using the following equation:

$$\alpha = \frac{4 * \pi * k}{\lambda} \quad (1)$$

Where λ is the wavelength and k is the extinction coefficient. The extracted data are used to calculate the optical absorption of both metal oxides (ZnO and Cu_2O) for each wavelength in the the following range [200 – 400 nm] and [250 – 650 nm) respectively. This is shown in **Figure 1**. The absorption depth is also important for the interpretation of the results as it reveals the thickness needed to absorb 60-65% of the incident radiation (**Figure 1)**.

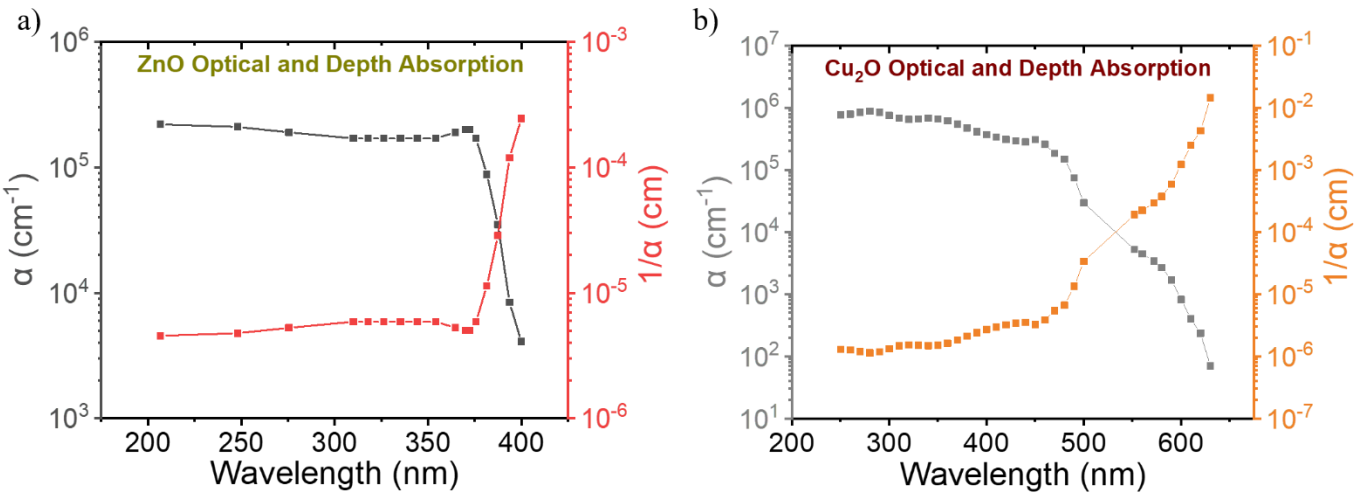

Figure 1. Optical absorption and the absorption depth (1/α) value for **(a)** ZnO and **(b)** Cu_2O respectively

Several material properties were also collected from literature, such as bandgap, electron affinity, electron thermal velocity, and density of states, in order to implement them to the software parameters. **Table 1** shows the parameters chosen for this particular study. These values have been compared with experimental results from other studies to follow the same range as the reported data[13,36,37]. In addition to these parameters, dopant concentrations have been included with a donor density of 10^{19} cm^{-3} for ZnO and an acceptor density of 10^{14} cm^{-3} for Cu_2O thin films. These values

were chosen based on average values found in the literature[38–41]. Additionally, defects were assumed to be neutral, since they are the ones that contribute the most to the Schockley-Read-Hall (SRH) recombination phenomena[31]. In this recombination model, the carrier lifetime is calculated using the following equation:

$$\tau = \frac{1}{\sigma_X N_t V_{th}} \quad (2)$$

Where N_t represents the defect density, V_{th}: 10^7 cm/s the thermal velocity, σ_X is the defect capture cross-section with σ_n : 10^{-14} cm^2 and σ_p : 10^{-15} cm^2 for Cu_2O and σ_n : 10^{-15} cm^2 and σ_p : 10^{-14} cm^2 for ZnO[42].

Table 1. Summary of the Properties of the Materials included in the numerical simulation work

Material Properties	**Values for ZnO Thin Film**	**References ZnO**	**Values for Cu_2O Thin Film**	**References Cu_2O**
Bandgap (eV)	3.4	*Borysiewicz, M. A. et al.*[43]	2.1	*Malerba, C. et al.*[34]
Electron Affinity (eV)	4.2	*McCluskey, M. D. et al.*[44]	3.2	*Nakano, Y. et al.* [45]
Dielectric Permittivity (relative)[34,46]	9	*Shetti, N. P. et al.*[46]	7.6	*Malerba, C. et al.*[34]
Conduction Band Density of States *(cm^{-3})*	2.2×10^{18}	*Ahmad, S. et al.*[47]	2.43×10^{19}	*Brandt, R. E. et al.*[48]
Valence Band Density of States *(cm^{-3})*	1.8×10^{19}		1.1×10^{19}	
Electron Thermal Velocity (cm/s)[49–51]	1.0×10^7	*Schmidt-Mende, L. et al.*[51]	1.0×10^7	*Biccari, F. et al.*[49] *Han, S. et al.*[50]
Hole Thermal Velocity (cm/s)[49–51]	1.0×10^7		1.0×10^7	
Electron Mobility (cm^2/Vs)	60	*Borysiewicz, M. A. et al.*[43]	100	*Biccari, F. et al.*[49] *Han, S. et al.*[50]
Hole Mobility (cm^2/Vs)	30		50	

The lifetime value is then used to calculate the diffusion length that is the squared product of diffusivity and lifetime[52]. Another important parameter that needs to be fixed is the distribution of the defects in the bandgap. For our study, we have chosen the Gaussian model for defect distribution, as it is commonly used to model the transport of layer defects in simulated solar cells[53]. All carrier lifetimes, defect concentration, and diffusion lengths used have been summarized in **Table 2.**

Table 2. Summary of the Defect Properties of the investigated Thin Film

Recombination Parameters	**ZnO**	**Cu_2O**
Carrier Lifetime (ns)	τ_n:0.1 / τ_p:0.01	τ_n:5 / τ_p:50
Diffusion Length (μm)	L_n:0.08/L_p:0.04	L_n:0.9/L_p:1
Carrier Diffusivity (cm^2/s)	D_n:0.64/D_p:1.6	D_n:1.62/D_p:0.25
Bulk Defect Density (cm^{-3})	10^{18}	2.10^{15}

3. RESULTS & DISCUSSION

The architecture of the simulated device is shown in **Figure 2.a** with an initial Cu_2O thickness of 2 μm in red and 0.1 μm for the ZnO thin film in blue. The illumination side in this case is through the ZnO layer, as commonly done in experimental studies.The calculated JV plot, shown in **Figure 2.a**, corresponds to an efficiency (η) of 6.67 %, an open circuit voltage (V_{oc}) of 1.093 V, a short-circuit current density (J_{sc}) of 9.85 mA/cm², and a fill factor (FF) of 61.96 %.

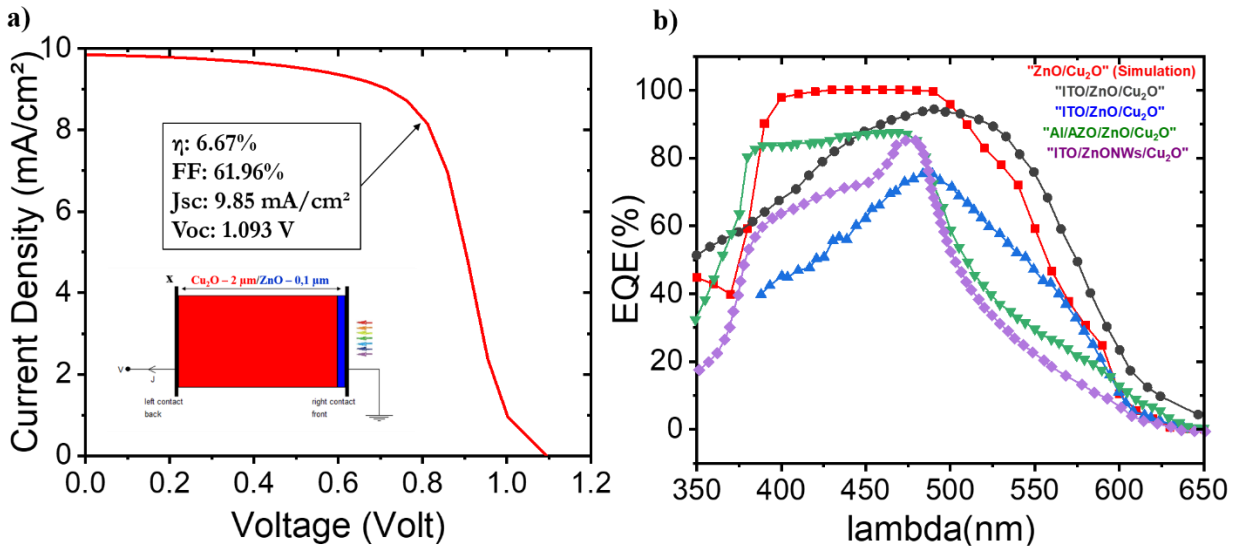

Figure 2. (a) Structure of the ZnO and Cu_2O stack device and Current-Voltage JV curve of the ZnO/Cu_2O device simulated in this study, and (b) external quantum efficiency of the device, along with several EQE from experimental studies in the literature for comparison.[4,12,33,54] The film thicknesses of the Cu_2O and ZnO layers are defined according to the color of the curve (Red: 2 µm-thick Cu_2O and 0.1 µm-thick ZnO, black: 170 µm-thick Cu_2O and 0.2 µm-thick ZnO, blue: 0.127 µm-thick Cu_2O and 0.15 µm-thick ZnO, green: 2.5 µm-thick Cu_2O and 0.05 µm-thick ZnO, and purple: 3 µm-thick Cu_2O and 1.25 µm-thick ZnO)

A small shoulder on the right part of the curve appears and is generally attributed to different band alignment at the junction and contacts within the structure (see previous simulation results by Y.Takiguchi *et al.*[22] for similar junctions while including a supplementary ZnO:Al layer on top of the ZnO). The JV output results of experimental devices based on ZnO/Cu_2O are summarized in **Supplementary Table 1.** The obtained Voc and Jsc are in the range of (0.3-0.65 V) and (4.4 – 11.42 mA/cm²) respectively[4,12,33,54]. The values of the current densities are within the range of the numerical simulation while the efficiency still shows poor performance (0.47 - 3.17 %) when compared to numerical simulation. **Figure 2.b** shows the external quantum efficiency (EQE)

obtained from the simulations (red curve). The maximum EQE values correspond to the wavelength range between 400 and 500 nm, where the absorption coefficient of Cu_2O is higher. As shown in **Figure 1.b**, the Cu_2O thickness is sufficient to convert most of the incident light to collected charge carriers. When comparing with experimental EQEs obtained from the literature, one can see that there is a high variation in terms of EQEs values and shape of the curve obtained for the different cells. Structures based only on ITO/ZnO/Cu_2O thin films (black and blue curves) show relatively high EQEs in the wavelength between 400 and 550 nm, whereas the addition of the AZO layer between ITO and ZnO layers (green curve) shows higher EQEs in the UV part of the spectrum (375 to 400 nm). Furthermore, the EQEs of Cu_2O thin films combined with ZnO nanowires show low values compared to the thin film-based structures for lower wavelengths. These differences in EQEs imply that different limiting factors are at play in the different cells studied in the cited references.

To try to understand the effect of the different parameters in the cell performance, mainly on the JV curve and the EQE, different parameters are varied in our simulations. First, the Cu_2O thickness is varied from 0.15 to 3.1 μm. **Figure 3.** presents the obtained JV curves and EQEs for the different thicknesses and the evolution of Jsc, Voc, η and FF versus thickness. It is clear to see that thicker layers result in higher Jsc values. The increase becomes less important as the thickness increases, tending to a maximum Jsc value above 10 mA/cm^2 for Cu_2O thickness values beyond 3 microns. Instead, the V_{oc} is noticed to decrease in an opposite trend with respect to the thickness of the absorber (see **Figure 3.c**). This is caused by the increase in charge recombination while increasing the thickness. This leads to a rise of the saturation current J_0 and thus induces a reduction of the V_{oc}[55].

Figure 3.b shows the EQEs for different Cu_2O thicknesses. As expected from the absorption coefficient of Cu_2O, and already seen in **Figure 2.b**, EQEs are maximum between 420 and 500 nm for low Cu_2O thicknesses, since these are the regions where Cu_2O absorbs more efficiently. Increasing the thickness has a strong impact on the EQE at longer wavelengths (in particular from 530 to 650 nm) that show a significant increase between 0.85 and 1.9 microns, beyond which only a minimal increase is obtained. The lower absorption of Cu_2O for wavelengths longer than 475 nm results thus in the need of thicker Cu_2O to maximize the amount of light absorbed, but the EQE values obtained above this wavelength are also affected by a limited charge diffusion length that results in recombination, and thus the EQE values show a decreasing trend as the wavelength increases. This incompatibility between absorption and collection depth has also been observed experimentally by A. Marin *et al.*[5].

Figure 3.c shows the variation of the output results (η, J_{sc}, and FF) with respect to the Cu_2O thickness. Those parameters reveal a sharp increase with the thickness of the Cu_2O film. This is mainly attributed to the increase in the absorption of the film and therefore to the current density and maximum power point. This affects significantly the fill factor and the efficiency of the device.

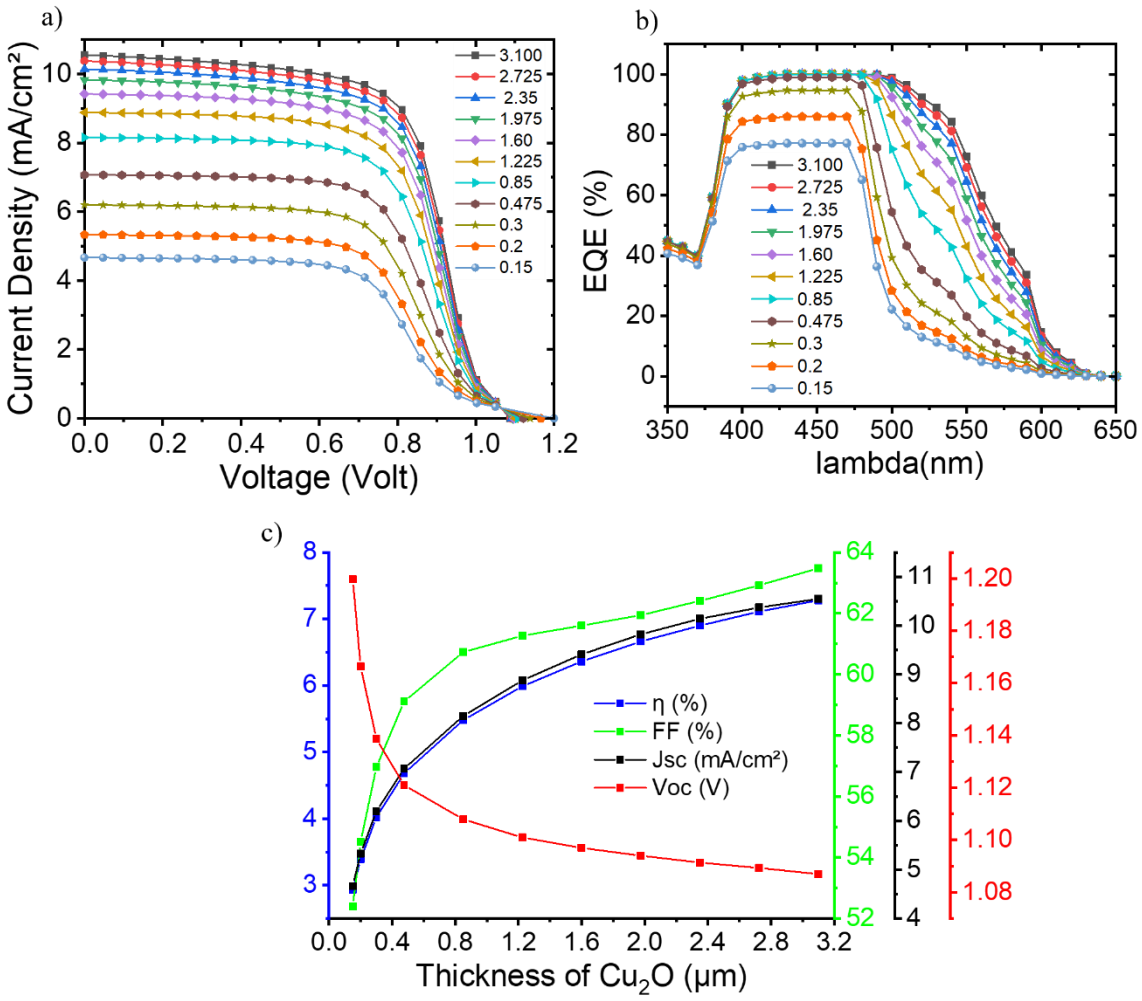

Figure 3. (a) JV curves and (b) EQEs and (c) Cell output parameters (V_{oc}, J_{sc}, FF, η) for different Cu_2O thicknesses ranging from 0.15 µm to 3.1 µm. – The diffusion length is 1 µm in all cases

Indeed, it is known that charge diffusion length plays a key role in charge recombination and, thus, the efficiency of solar cells. To evaluate the impact of this parameter in ZnO/Cu_2O devices, we performed simulations varying the diffusion length from 0.01 to 15 µm for Cu_2O (keeping the other initial parameters unchanged, i.e. 2 µm thick Cu_2O and 0.1 µm thick ZnO, and optical parameters detailed in **Figure 1**). **Figure 4.a** shows the JV curves of the junction with varied diffusion length and degradation of the output cell parameters is observed, mainly (η, J_{sc}, and FF),

for the lower diffusion lengths. The V_{oc} decreases slightly with the increase of the diffusion length as shown in the evolution of the output results versus diffusion length (**Supplementary Figure 1**). This evolution confirms the effect of recombination that becomes predominant by reducing the diffusion length. This is also revealed in **Figure 4.b** in which the variation of the EQEs is quite apparent for the whole spectra. Below 2 µm, the EQE begins to decrease progressively at wavelengths above 500 nm. This is more apparent by further reducing the diffusion length to 0.1 µm as the EQE shows a significant decrease above 400 nm. It is interesting to mention that beyond 2 µm, which corresponds to the Cu_2O film thickness in the reference cell, the evolution of the output parameters is relatively small. The study shows that a smaller diffusion length of minority carriers compared to solar cell thicknesses induces a significant increase of the recombination and decrease of the efficiency.

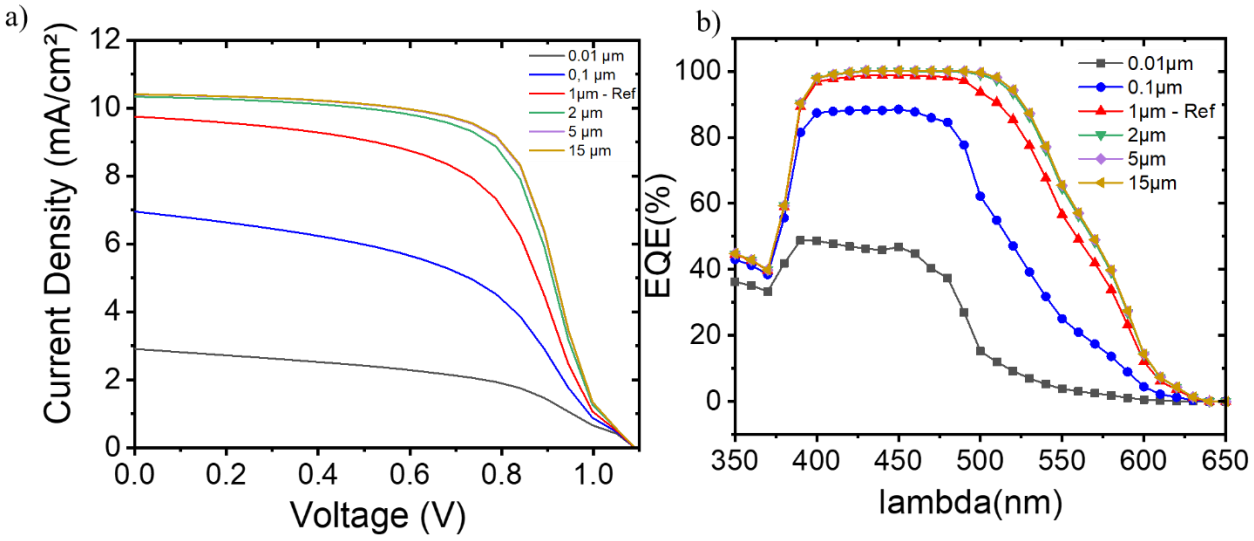

Figure 4. (a) Current-voltage JV curve of the simulated ZnO/Cu_2O device, and **(b)** external quantum efficiency of the device stack, for different diffusion lengths of Cu_2O (0.01 µm to 15 µm)

Apart from Cu_2O thickness and diffusion length, the thickness of the ZnO is also an important parameter that needs to be considered and varied towards understanding its impact on the device performance (also since different thicknesses are often used in experimental reports). Therefore, simulations were performed with varying ZnO thickness from 30 to 200 nm (**Figure 5**). **Figure 5.a** shows the JV curves obtained, where Jsc shows a slight increase as the ZnO thickness decreases. Conversely, V_{oc} remains the same, while the FF shows a mild decrease of less than 1% (see **Figure 5.c**). The EQEs obtained are presented in **Figure 5.b**, and an increase at lower wavelengths can be observed with decreasing ZnO thickness. Thus, thicker ZnO layers result in a slight decrease in cell efficiency mainly due to a decrease in Jsc and FF. The explanation behind this variation is the increase of the recombination induced by the thicker ZnO layer compared to its minority carrier diffusion length of 0.04 μm. Therefore, the conclusion from this study is that the thickness of ZnO layer needs to be reduced as much as possible. In fact, due to its short diffusion length of charge carriers and low absorption coefficient in the visible wavelength range, recombination is the main limiting phenomena when varying the thickness of ZnO.

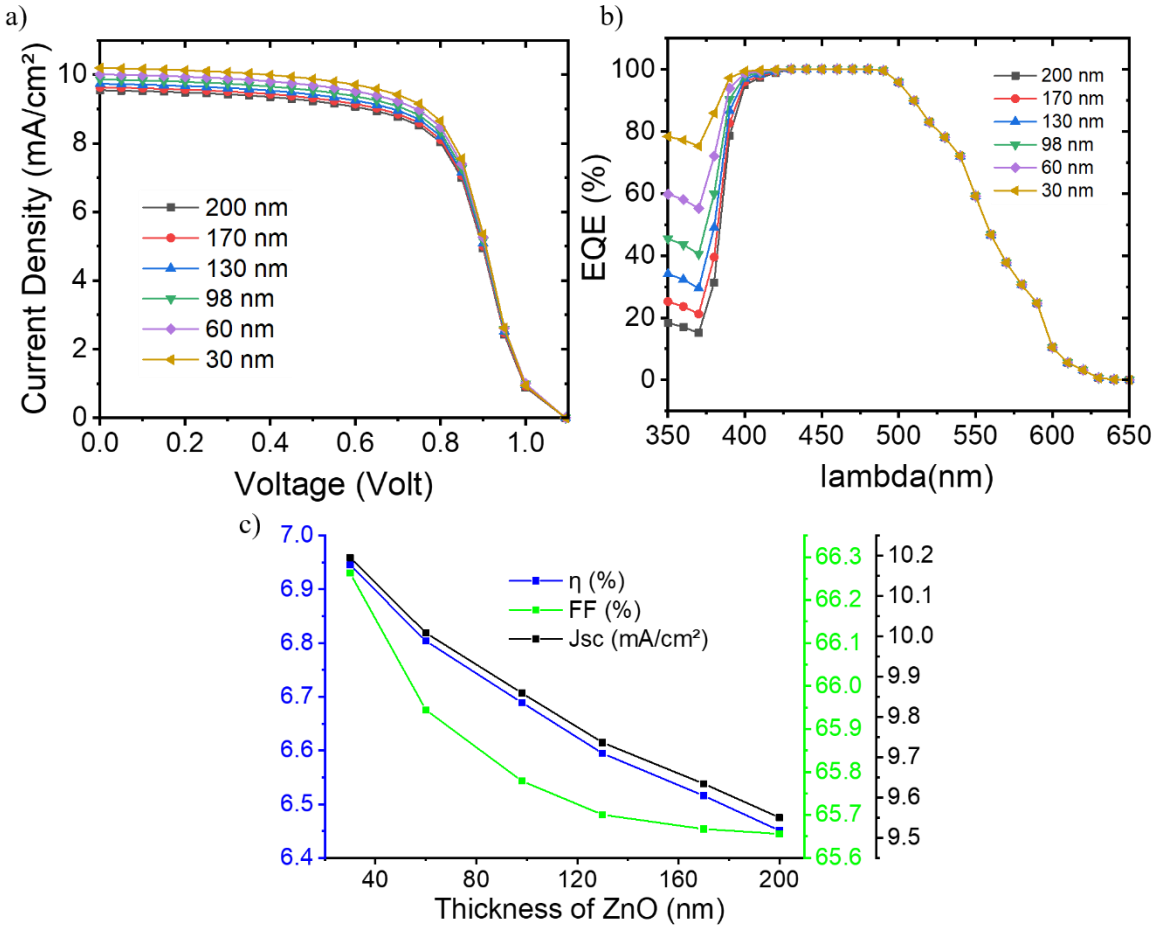

Figure 5. (a) Current-voltage JV curve of the simulated ZnO/Cu_2O device, **(b)** external quantum efficiency, and **(c)** output results of the device stack (J_{sc}, FF, η) with different ZnO thicknesses varying from 30 to 200 nm

So far, all simulation results have been obtained for a solar cell that is illuminated from the ZnO side (see **Figure 2.a**). This configuration is usually used in experimental studies since in this way carriers are generated near the junction and thus cell efficiency is less affected by limited electron diffusion length in Cu_2O. But from the simulation point of view, it is interesting to explore the possibility to illuminate the cell from the Cu_2O side or even from both sides (i.e. bifacial

illumination, as done for other systems). As a first approach, the illumination from the Cu_2O side was performed with a Cu_2O thickness of 2 µm. In this case, the simulation did not converge since the diffusion length (1 µm) is lower with respect to the film thickness used and the defects present in Cu_2O would induce recombination of the generated charges, which thus does not allow a proper charge collection (**Figure 6.c.i)**. The thickness of Cu_2O was thus reduced to 0.8 µm and 0.5 µm and a reduction in the JV curve with respect to the illumination through the ZnO side for equivalent devices was observed, as shown in **Figure 6.a**. This is also confirmed by the EQE shown in **Figure 6.b** since, at wavelengths below 475 nm, the photons are absorbed near the surface when illuminating from the Cu_2O side (**Figure 6.c.ii)**. The minority carriers have a greater distance to diffuse through to the depletion layer, and thus a smaller thickness is suitable while inducing illumination from this side to avoid recombination. Above 475 nm, the carriers are generated deeper and, therefore, closer to the depletion region, which increases their probability to be collected. On the other hand, the bi-facial illumination shows a high and constant EQE between 350 nm and 530 nm. In this case, the quantum efficiency is taken from both sides (ZnO & Cu_2O), which explains the high values obtained. Further, the EQE follows a gradual decrease above 530 nm.

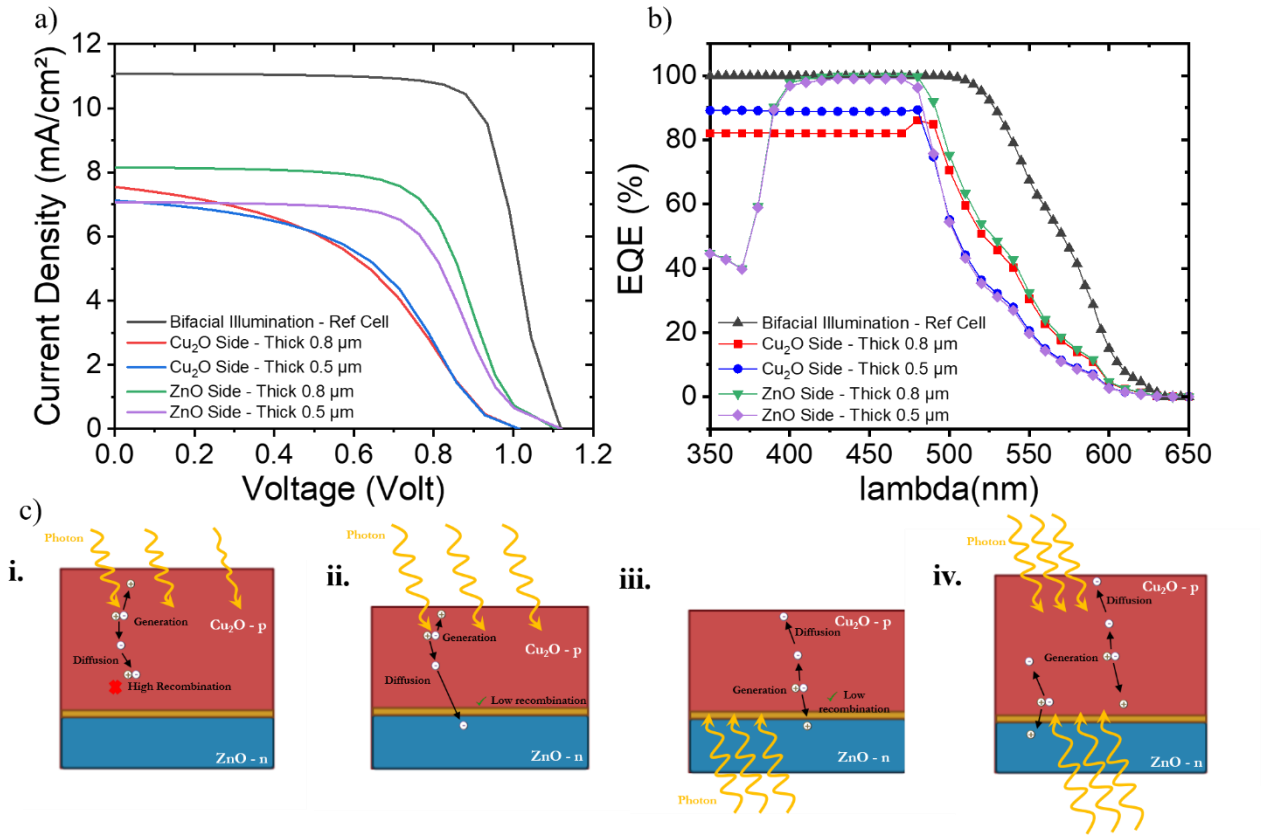

Figure 6. (a) Current-Voltage JV curve, and **(b)** EQEs of the device stack, with different side and bifacial illumination, and **(c)** schematic of the charge separation mechanism of a typical solar cell illuminated from Cu_2O (Red color) with thickness of **i.** 2 µm, or **ii.** 0.5-0.8 µm, from the **iii.** ZnO side (Blue color) with (0.5-0.8 µm Cu_2O thick) and ZnO (0.1 µm thick), and from **iv.** both sides; Cu_2O (Blue color) with 2 µm thick and ZnO (0.1 µm thick)

Table 3 summarizes the output results for different side illuminations and demonstrates that the efficiency is slightly lower when illuminated from the Cu_2O side. However, the FF decreases significantly, with a difference of about 15 %. This can be explained by the fact that the generated carriers have a longer distance to travel before reaching the depletion region and would induce more recombination through their motion. The bifacial illumination shows an improved output

performances and results very appealing for semitransparent devices that could be used for indoor light harvesting or in semitransparent windows (where light could be collected from out and indoors)[13].

Table 3. Summary of the Output Results with different side and bifacial illumination

Structures	η (%)	FF (%)	J_{sc} (mA/cm²)	V_{oc} (V)
Bifacial Illumination – 2µm Cu_2O	9.20	74.37	11.07	1.1178
Illuminated from Cu_2O – 0.8 µm	3.32	42.190	7.547	1.013
Illuminated from Cu_2O – 0.5 µm	3.36	46.45	7.124	1.015
Illuminated from ZnO – 0.8 µm	5.48	60.73	8.15	1.107
Illuminated from ZnO – 0.5 µm	4.68	59.11	7.07	1.121

As mentioned in the first part of this section, all of the studies performed were done without taking into account defects at the interfaces. But indeed experimental results show that the nature and quality of the interface are very important to maximize the obtained efficiency[14,56,57]. Particular attention was paid to this parameter since different phenomena could occur in this part of the cell and cause recombination of the charges and prevent their collection. We have thus explored the effect of introducing defects at the junction interface to evaluate the effect on the efficiency. There are not much data in the literature on these types of defects and their concentrations, especially for the ZnO/Cu_2O interface. SCAPS software uses a thermionic emission model that is integrated for the interface transport properties. The recombination mechanism at the interface is modeled on the

basis of the Pauwel-Vanhoule theory, which is an extension of the Schockley-Read-Hall theory[31]. In view of this, neutral interface defects were assumed for our simulation since such types of defects contribute to the SRH recombination. The default capture cross section σ_n and σ_p were both set to be 10^{-13} cm^{-2} , which means the capture coefficient of interface states has the same probability for both electrons and holes[58]. Then the only unknown parameter is the defect concentration at the interface, and we will analyze its impact on device performance.

Figure 7.a and **Figure 7.b** present the JV curve and EQEs with different defect densities at the Cu_2O/ZnO interface. The Voc values decrease drastically for interface defect concentration going from 10^{10} cm^{-2} to 10^{13} cm^{-2} and then stabilize beyond this value. Unlike Jsc, Voc decreases significantly just after the introduction of defects at the interface to the reference cell, from 1.09 V to 0.77 V, and then continues to decrease slightly until it reaches 0.66 V (**Figure 7.c).** This has a direct impact on the FF and η of the device respectively**.** The quantum efficiency is impacted for wavelengths below 520 nm. J. Gan *et al.* have indeed observed that interfacial defects mostly impact the EQEs of short wavelengths[14]. This indicates the recombination generated at the Cu_2O surface defects that are triggered by the defects. The trend shows that as defect concentration increases, more recombination is induced at the depletion layer and, therefore, promotes degradation of the device performances.

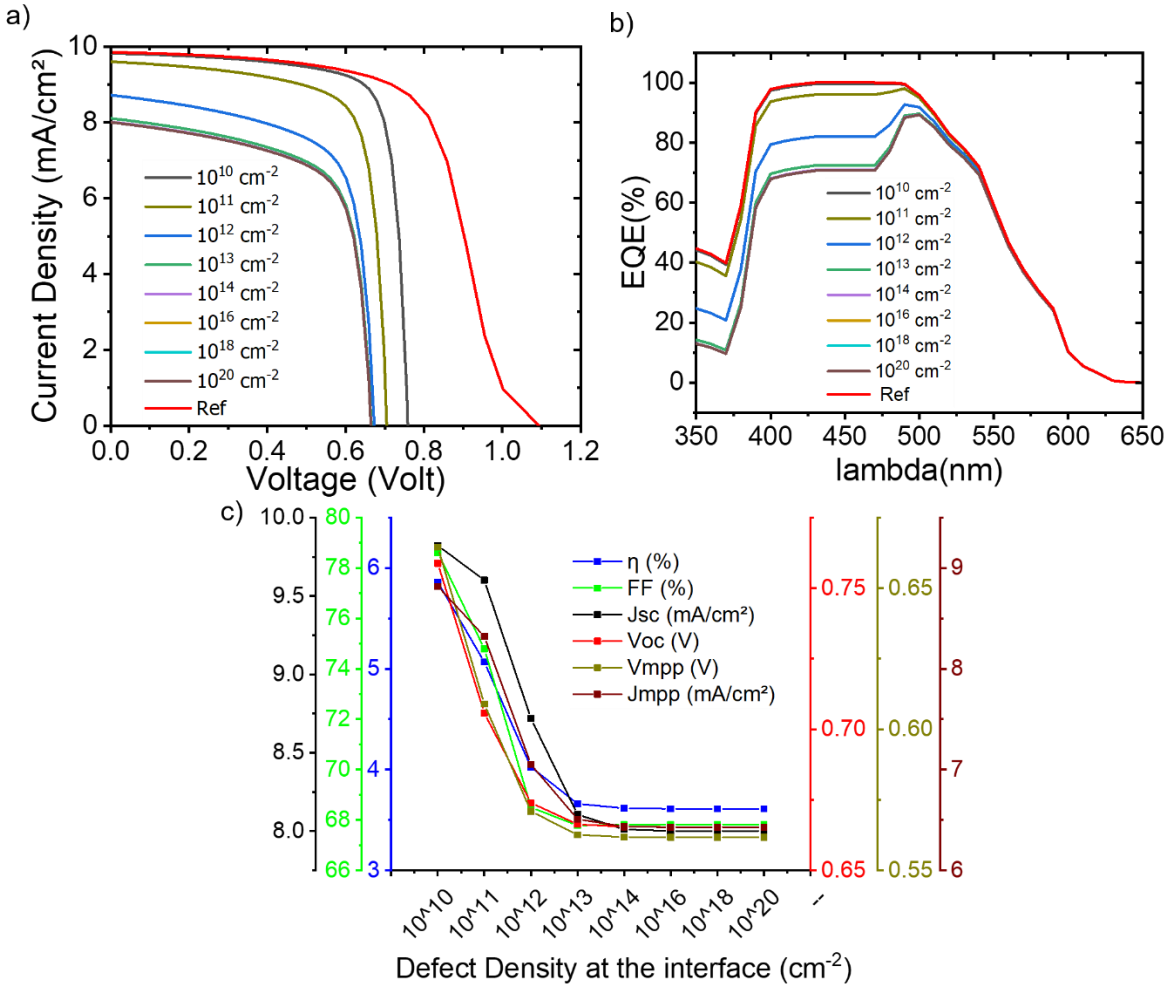

Figure 7. (a) Current-Voltage JV curve, **(b)** EQE, **(c)** output parameters of the device stack (V_{oc}, J_{sc}, FF, η, V_{mpp}, J_{mpp}) with different defect densities at the ZnO/Cu_2O interface.

Overall, we have shown in this study the impact of the different major parameters that could be modified to obtain higher results and understand their effect on the device physics. **Figure 8.a** shows the external quantum efficiency of the reference cell shown previously (**Figure 2**) with respect to experimental ZnO/Cu_2O solar cell reported in the literature[4,9,12,54] . *Ievskaya. Y, et al, Lee. Y. S, et al,* and *Z. Zang, et al* have demonstrated that oxidation of Cu_2O surface due to the post-annealing process induces defect at the interface and thus limits the output results[9,12,54]. *Z.*

Zang, et al have also shown that the orientation of the film improves the diffusion length and therefore the output performance of the cell[12]. The effect of these parameters is observed in the evolution of the EQEs in **Figure 8**.**a** with respect to the simulated results especially in the dark purple and grey regions**.** The absorber thickness plays an important role in the aforementioned two regions as demonstrated by the experimental results. As the Cu_2O thickness increases from 0.127 µm[9] to 170 µm[12], the EQE values increase at higher wavelengths. Additionally, when comparing the results from the experimental work reported in here, it is clear that the ZnO thickness plays also an important role and should be reduced as much as possible, as demonstrated by the enhanced EQEs in the study of *Lee. Y. S, et al.*[54] (ZnO ~0.05 µm), which confirms the simulation results obtained. Further, *Musselman. K. P,* et al have studied the obtained EQEs for Cu_2O combined with planar ZnO and nanowires[4]. The reported work demonstrated that the output results are limited by both diffusion length and interface recombination. Following this discussion, the data obtained are separated into three main sections: **I.** below 390 nm (light purple), **II.** 390 – 480 nm (dark purple), **III.** above 480 nm (grey). This separation will be useful to clarify the different phenomena that have been extracted from this study and that could considerably affect the value obtained for the ZnO/Cu_2O junction. Below 390 nm, most of the variation comes from the effect of ZnO thickness, interface defects, and lateral illumination, which alter the diffusion of charges across the junction. Above 390 nm, the variation in EQEs is mainly due to the thickness of Cu_2O and thus its absorption. In addition, there is a contribution from interfacial defects that may exist at the PN junction between 390 nm and 480 nm. Above 480 nm, the limited diffusion length of minority carrier in Cu_2O results detrimental (**Figure 8**.**b**)

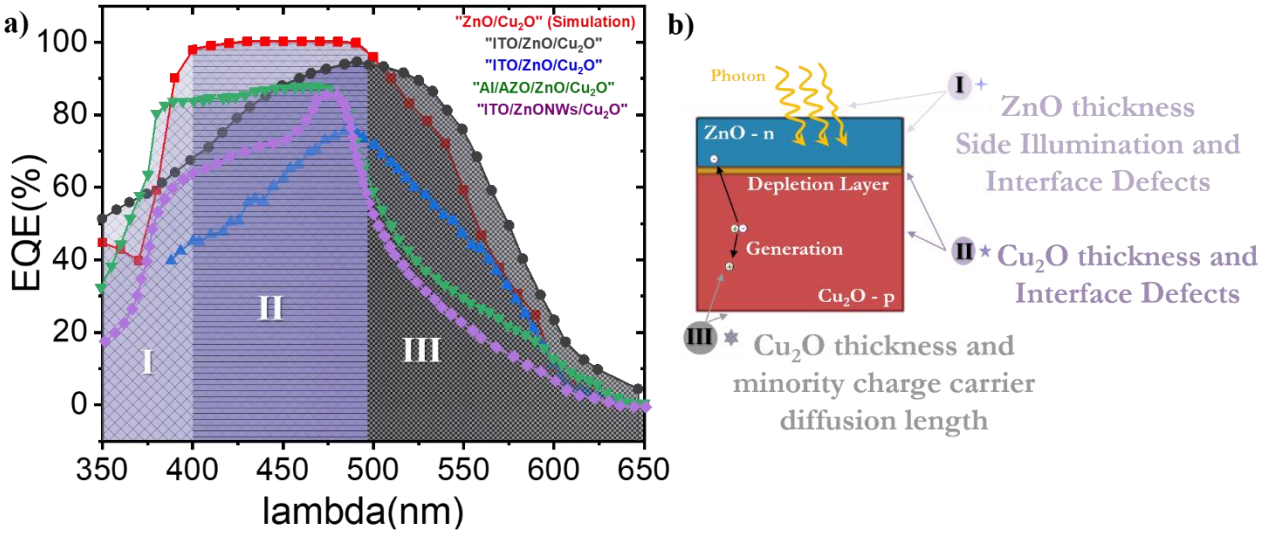

Figure 8. (a) The EQE curve of the reference samples with 0.1 µm thick ZnO and 2 µm thick Cu_2O and experimental solar cells based on Cu_2O and ZnO[4,12,33,54], separated in different slices and **(b)** schematic of the simulated parameters responsible for the changes in the quantum efficiency in the cell. The film thicknesses of the Cu_2O and ZnO layers are defined according to the color of the curve (Red: 2 µm-thick Cu_2O and 0.1 µm-thick ZnO, black: 170 µm-thick Cu_2O and 0.2 µm-thick ZnO, blue: 0.127 µm-thick Cu_2O and 0.15 µm-thick ZnO, green: 2.5 µm-thick Cu_2O and 0.05 µm-thick ZnO, and purple: 3 µm-thick Cu_2O and 1.25 µm-thick ZnO)

4. CONCLUSION

In summary, numerical simulations of simple ZnO/Cu_2O all-oxide solar cells (without doping or extra interfacial layers) were performed using the SCAPS software to identify the main parameters that affect the behavior of the cells, and correlate these to experimental results reported in the literature, with the aim to provide feasible routs toward efficiency optimization. The parameters studied are thickness variation for both Cu_2O and ZnO, minority carrier diffusion length for Cu_2O, side illumination (ZnO, Cu_2O, or bifacial), and the quality of the junction interface. This is the first

study in which bifacial illumination was implemented in the simulations with this software. The results show a clear enhancement in the efficiency of the cell when illuminated from both sides, and that thin semitransparent Cu_2O are very appealing for windows or even indoor light harvesting. Further, the variation in absorber and collector thickness proves to be a key to the output results, especially when coordinated with the diffusion length of the films. Nevertheless, defects present at the interface generate recombination and prevent proper charge collection. All these factors affect differently to the different regions of the EQE. Overall, this comprehensive study provides a *modus operandi* for understanding and eventually implementing our findings in the experimental work by adjusting the key parameters of the junction, so that efficiencies close to the theoretical values can be achieved for ZnO/Cu_2O all-oxide solar cells.

Supporting Information

The Supporting Information is available free of charge at

Output results of experimental and simulated results.

Corresponding Authors

Abderrahime Sekkat - Univ. Grenoble Alpes, CNRS, Grenoble INP, LMGP, F-38000 Grenoble, France. Univ. Grenoble Alpes, Univ. Savoie Mont Blanc, CNRS, Grenoble INP, IMEP-LaHC, 38000 Grenoble, France. Univ. Grenoble Alpes, CNRS, Grenoble INP, SIMAP, 38000 Grenoble, France. Email: abderrahime.sekkat@grenoble-inp.fr

David Muñoz-Rojas - Univ. Grenoble Alpes, CNRS, Grenoble INP, LMGP, F-38000 Grenoble, France. Email: david.munoz-rojas@grenoble-inp.fr

Anne Kaminski-Cachopo - Univ. Grenoble Alpes, Univ. Savoie Mont Blanc, CNRS, Grenoble INP, IMEP-LaHC, 38000 Grenoble, France. Email: anne.kaminski@grenoble-inp.fr

Authors

Daniel Bellet - Univ. Grenoble Alpes, CNRS, Grenoble INP, LMGP, F-38000 Grenoble, France. Email: Daniel.Bellet@grenoble-inp.fr

Guy Chichignoud - Univ. Grenoble Alpes, CNRS, Grenoble INP, SIMAP, 38000 Grenoble, France. Email: guy.chichignoud@grenoble-inp.fr

ACKNOWLEDGMENT

This work has been partially supported by the CDP Eco-SESA receiving funds from the French National Research Agency in the framework of the "Investments for the future" program (ANR-15-IDEX-02). DMR acknowledges the support of the Horizon 2020 FETOPEN-1-2016-2017 research and innovation program of the European Union under Grant Agreement 801464, and through Marie Curie Actions (FP7/2007-2013, Grant Agreement No. 63111). The authors thank the Agence Nationale de la Recherche (ANR, France) via the DESPATCH project (No. ANR-16-CE05-0021) and Carnot energies du future. The authors warmly thank Prof. Marc Burgelman for fruitful discussions, for providing us with the SCAPS-1D software, and for helping us set the bifacial illumination for this study.

REFERENCES

(1) Meyer, B. K.; Polity, A.; Reppin, D.; Becker, M.; Hering, P.; Kramm, B.; Klar, P. J.; Sander, T.; Reindl, C.; Heiliger, C.; Heinemann, M.; Müller, C.; Ronning, C. *Chapter Six – The Physics of Copper Oxide (Cu_2O)*; 2013; Vol. 88.

(2) Olsen, L. C.; Addis, F. W.; Miller, W. Experimental and Theoretical Studies of Cu_2O Solar

Cells. *Sol. Cells* **1982**, *7* (3), 247–279.

(3) Scanlon, D. O.; Watson, G. W. Undoped N-Type Cu_2O: Fact or Fiction? *J. Phys. Chem. Lett.* **2010**, *1* (17), 2582–2585.

(4) Musselman, K. P.; Wisnet, A.; Iza, D. C.; Hesse, H. C.; Scheu, C.; MacManus-Driscoll, J. L.; Schmidt-Mende, L. Strong Efficiency Improvements in Ultra-Low-Cost Inorganic Nanowire Solar Cells. *Adv. Mater.* **2010**, *22* (35), 254–258.

(5) Marin, A. T.; Muñoz-Rojas, D.; Iza, D. C.; Gershon, T.; Musselman, K. P.; MacManus-Driscoll, J. L. Novel Atmospheric Growth Technique to Improve Both Light Absorption and Charge Collection in ZnO/Cu_2O Thin Film Solar Cells. *Adv. Funct. Mater.* **2013**, *23* (27), 3413–3419.

(6) Chala, S.; Boumaraf, R.; Bouhdjar, A. F.; Bdirina, M.; Labed, M.; Taouririt, T. E.; Elbar, M.; Sengouga, N.; Yakuphanoğlu, F.; Rahmane, S.; Naoui, Y.; Benbouzid, Y. Synthesis and Characterization of ZnO Thin Film for Modeling the Effect of Its Defects on ZnO/Cu_2O Solar Cell EQE. *J. Nano- Electron. Phys.* **2021**, *13* (1), 1–6.

(7) Jacobsen, E. C. Analysis of the ZnO/Cu_2O Thin Film Heterojunction for Intermediate Band Solar Cell Applications. **2015**, No. June, 105.

(8) Jeong, S. S.; Mittiga, A.; Salza, E.; Masci, A.; Passerini, S. Electrodeposited ZnO/Cu_2O Heterojunction Solar Cells. *Electrochim. Acta* **2008**, *53* (5), 2226–2231.

(9) Ievskaya, Y.; Hoye, R. L. Z.; Sadhanala, A.; Musselman, K. P.; MacManus-Driscoll, J. L. Fabrication of ZnO/Cu_2O Heterojunctions in Atmospheric Conditions: Improved Interface Quality and Solar Cell Performance. *Sol. Energy Mater. Sol. Cells* **2015**, *135*, 43–48.

(10) Ievskaya, Y.; Hoye, R. L. Z.; Sadhanala, A.; Musselman, K. P.; MacManus-Driscoll, J. L. Improved Heterojunction Quality in Cu_2O-Based Solar Cells Through the Optimization of Atmospheric Pressure Spatial Atomic Layer Deposited $Zn_{1-X}Mg_xO$. *J. Vis. Exp.* **2016**, No. 113, 1–7.

(11) Fujimoto, K.; Oku, T.; Akiyama, T. Fabrication and Characterization of ZnO/Cu_2O Solar

Cells Prepared by Electrodeposition. *Appl. Phys. Express* **2013**, *6* (8), 086503.

(12) Zang, Z. Efficiency Enhancement of ZnO/Cu_2O Solar Cells with Well Oriented and Micrometer Grain Sized Cu_2O Films. *Appl. Phys. Lett.* **2018**, *112* (4), 086503.

(13) Sekkat, A.; Nguyen, V. H.; Arturo, C.; La, M. De; Rapenne, L.; Bellet, D.; Kaminski-cachopo, A.; Chichignoud, G.; Muñoz-rojas, D. Open-Air Printing of Cu_2O Thin Films with High Hole Mobility for Semitransparent Solar Harvesters. *Commun. Mater.* **2021**, *2*, 78.

(14) Gan, J.; Hoye, R. L. Z.; Ievskaya, Y.; Vines, L.; Marin, A. T.; MacManus-Driscoll, J. L.; Monakhov, E. V. Elucidating the Origin of External Quantum Efficiency Losses in Cuprous Oxide Solar Cells through Defect Analysis. *Sol. Energy Mater. Sol. Cells* **2020**, *209* (January 2020), 110418.

(15) Lei, Q.; Zhu, H.; Song, K.; Wei, N.; Liu, L.; Zhang, D.; Yin, J.; Dong, X.; Yao, K.; Wang, N.; Li, X.; Davaasuren, B.; Wang, J.; Han, Y. Investigating the Origin of Enhanced C^{2+} Selectivity in Oxide-/Hydroxide-Derived Copper Electrodes during CO_2 Electroreduction. *J. Am. Chem. Soc.* **2020**, *142* (9), 4213–4222.

(16) Ru, S.; Anderson, A. Y.; Barad, H.; Kupfer, B.; Bouhadana, Y.; Rosh-hodesh, E.; Zaban, A. All-Oxide Photovoltaics. *J. Phys. Chem. Lett.* **2012**, *3*, 3755–3764.

(17) Dumitru, C.; Muscurel, V.-F.; Fara, L. Cu_2O Layer Analysis and Optimization Based on a Metal-Oxide Tandem Heterojunction Solar Cell. *Mater. Today Proc.* **2018**, *5* (8), 15895–15901

(18) Siol, S.; Hellmann, J. C.; Tilley, S. D.; Graetzel, M.; Morasch, J.; Deuermeier, J.; Jaegermann, W.; Klein, A. Band Alignment Engineering at Cu_2O/ZnO Heterointerfaces. *ACS Appl. Mater. Interfaces* **2016**, *8* (33), 21824–21831.

(19) Lam, N. D. Modelling and Numerical Analysis of ZnO/CuO/Cu_2O Heterojunction Solar Cell Using SCAPS. *Eng. Res. Express* **2020**, *2* (2), 025033.

(20) Nordseth, Ø.; Kumar, R.; Bergum, K.; Fara, L.; Foss, S. E.; Haug, H.; Drăgan, F.; Crăciunescu, D.; Sterian, P.; Chilibon, I.; Vasiliu, C.; Baschir, L.; Savastru, D.; Monakhov,

E.; Svensson, B. G. Optical Analysis of a ZnO/Cu_2O Subcell in a Silicon-Based Tandem Heterojunction Solar Cell. *Green Sustain. Chem.* **2017**, *07* (01), 57–69.

(21) Chevallier, C.; Bose, S.; Ould Saad Hamady, S.; Fressengeas, N. Numerical Investigations of the Impact of Buffer Germanium Composition and Low Cost Fabrication of Cu_2O on AZO/ZnGeO/Cu_2O Solar Cell Performances. *EPJ Photovoltaics* **2021**, *12*.

(22) Takiguchi, Y.; Miyajima, S. Device Simulation of Cuprous Oxide Heterojunction Solar Cells. *Jpn. J. Appl. Phys.* **2015**, *54* (11), 112303.

(23) Fentahun, D. A.; Tyagi, A.; Kar, K. K. Numerically Investigating the AZO/Cu_2O Heterojunction Solar Cell Using ZnO/CdS Buffer Layer. *Optik (Stuttg).* **2021**, *228* (May 2020), 166228.

(24) Rizi, M. T.; Shahrokh Abadi, M. H. Numerical Investigation on Efficiency Improvement of Double Layer Antireflection Coating AZO/Buffer/Cu_2O/CuO on Back-Surface Fluorine-Doped Tin Oxide Heterostructure Solar Cells. *J. Opt. Soc. Am. B* **2019**, *36* (4), 1155.

(25) Sawicka-Chudy, P.; Starowicz, Z; Wisz, G.; Yavorskyi, R.; Zapukhlyak, Z.; Bester, M.; Glow, L.; Sibinski, M.; Cholewa, M. Simulation of TiO_2/CuO Solar Cells with SCAPS-1D Software. *Mater. Res. Express* **2019,** 6, 085912.

(26) Tauc, J.; Menth, A. States in the Gap. *J. Non. Cryst. Solids* **1972**, *8–10* (C), 569–585.

(27) Simya, O. K.; Mahaboobbatcha, A.; Balachander, K. A Comparative Study on the Performance of Kesterite Based Thin Film Solar Cells Using SCAPS Simulation Program. *Superlattices Microstruct.* **2015**, *82*, 248–261.

(28) Liu, Y.; Sun, Y.; Rockett, A. A New Simulation Software of Solar Cells - wxAMPS. *Sol. Energy Mater. Sol. Cells* **2012**, *98*, 124–128.

(29) Morales-Acevedo, A. Design of Very Thin CdTe Solar Cells with High Efficiency. *Energy Procedia* **2014**, *57*, 3051–3057.

(30) Toghyani Rizi, M.; Shahrokh Abadi, M. H.; Ghaneii, M. Two Dimensional Modeling of

Cu_2O Heterojunction Solar Cells Based-on β-Ga_2O_3 Buffer. *Optik (Stuttg).* **2018**, *155*, 121–132.

(31) Burgelman, M.; Nollet, P.; Degrave, S. Modelling Polycrystalline Semiconductor Solar Cells. *Thin Solid Films* **2000**, *361*, 527–532.

(32) Clugston, D. A.; Basore, P. A. PC1D Version 5: 32-Bit Solar Cell Modeling on Personal Computers. *Conf. Rec. IEEE Photovolt. Spec. Conf.* **1997**, 207–210.

(33) Hoye, R. L. Z.; Brandt, R. E.; Ievskaya, Y.; Heffernan, S.; Musselman, K. P.; Buonassisi, T.; Macmanus-Driscoll, J. L. Perspective: Maintaining Surface-Phase Purity Is Key to Efficient Open Air Fabricated Cuprous Oxide Solar Cells. *APL Mater.* **2015**, *3* (2), 020901.

(34) Malerba, C.; Biccari, F.; Leonor Azanza Ricardo, C.; D'Incau, M.; Scardi, P.; Mittiga, A. Absorption Coefficient of Bulk and Thin Film Cu_2O. *Sol. Energy Mater. Sol. Cells* **2011**, *95* (10), 2848–2854.

(35) Stelling, C.; Singh, C. R.; Karg, M.; König, T. A. F.; Thelakkat, M.; Retsch, M. Plasmonic Nanomeshes: Their Ambivalent Role as Transparent Electrodes in Organic Solar Cells. *Sci. Rep.* **2017**, *7* (September 2016), 1–13.

(36) Nguyen, V. S.; Sekkat, A.; Bellet, D.; Chichignoud, G.; Kaminski-cachopo, A.; Muñoz-Rojas, D.; Favre, W.; Muñoz-Rojas, and D.; Favre, W. Open-Air, Low-Temperature Deposition of Phase Pure Cu_2O Thin Films as Efficient Hole-Transporting Layers for Silicon Heterojunction Solar Cells. *J. Mater. Chem. A* **2021**, *9* (10.1039/D1TA02931B), 15968–15974.

(37) de la Huerta, C. A. M.; Nguyen, V. H.; Sekkat, A.; Crivello, C.; Toldra-Reig, F.; Veiga, P. B.; Quessada, S.; Jimenez, C.; Muñoz-Rojas, D. Gas-Phase 3D Printing of Functional Materials. *Adv. Mater. Technol.* **2020**, *2000657*, 1–8.

(38) Vyas, S. A Short Review on: Optimization Techniques of ZnO Based Thin Film Transistors. *Chinese J. Phys.* **2018**, *56* (1), 117–124.

(39) Al-Jawhari, H. A. A Review of Recent Advances in Transparent p-Type Cu_2O-Based Thin

Film Transistors. *Mater. Sci. Semicond. Process.* **2015**, *40*, 241–252.

(40) Rai, B. P. Cu_2O Solar Cells:A Review. *Sol. Cells* **1988**, *25*, 265–272.

(41) Wang, Y.; Pierson, J. F. Binary Copper Oxides as Photovoltaic Absorbers: Recent Progress in Materials and Applications. *J. Phys. D. Appl. Phys.* **2021**, *54* (26), 263002.

(42) Zhu, L.; Shao, G.; Luo, J. K. Numerical Study of Metal Oxide Hetero-Junction Solar Cells with Defects and Interface States. *Semicond. Sci. Technol.* **2013**, *28* (5), 055004.

(43) Borysiewicz, M. A. ZnO as a Functional Material, a Review. *Crystals* **2019**, *9* (10), 505.

(44) McCluskey, M. D.; Jokela, S. J. Defects in ZnO. *J. Appl. Phys.* **2009**, *106* (7), 071101.

(45) Nakano, Y.; Saeki, S.; Morikawa, T. Optical Bandgap Widening of p -Type Cu_2O Films by Nitrogen Doping. *Appl. Phys. Lett.* **2009**, *94* (2), 1–4.

(46) Shetti, N. P.; Bukkitgar, S. D.; Reddy, K. R.; Reddy, C. V.; Aminabhavi, T. M. ZnO-Based Nanostructured Electrodes for Electrochemical Sensors and Biosensors in Biomedical Applications. *Biosens. Bioelectron.* **2019**, *141* (March), 111417.

(47) Ahmad, S.; Abbas, H.; Bilal Khan, M.; Nagal, V.; Hafiz, A. K.; Khan, Z. H. ZnO for Stable and Efficient Perovskite Bulk Heterojunction Solar Cell Fabricated under Ambient Atmosphere. *Sol. Energy* **2021**, *216* (September 2020), 164–170.

(48) Brandt, R. E.; Young, M.; Park, H. H.; Dameron, A.; Chua, D.; Lee, Y. S.; Teeter, G.; Gordon, R. G.; Buonassisi, T. Band Offsets of n-Type Electron-Selective Contacts on Cuprous Oxide (Cu_2O) for Photovoltaics. *Appl. Phys. Lett.* **2014**, *105* (26), 263901.

(49) Biccari, F. Defects and Doping in Cu_2O. *Solid State Commun.* **2009**, No. 688774, 262.

(50) Han, S.; Flewitt, A. J. Analysis of the Conduction Mechanism and Copper Vacancy Density in p-Type Cu_2O Thin Films. *Sci. Rep.* **2017**, *7* (1), 1–8.

(51) Schmidt-Mende, L.; MacManus-Driscoll, J. L. ZnO - Nanostructures, Defects, and Devices. *Mater. Today* **2007**, *10* (5), 40–48.

(52) Özgür, Ü.; Alivov, Y. I.; Liu, C.; Teke, A.; Reshchikov, M. A.; Doğan, S.; Avrutin, V.; Cho, S. J.; Morkǫ, H. A Comprehensive Review of ZnO Materials and Devices. *J. Appl. Phys.* **2005**, *98* (4), 1–103.

(53) Goudarzi, M.; Banihashemi, M. Simulation of an Inverted Perovskite Solar Cell with Inorganic Electron and Hole Transfer Layers. *J. Photonics Energy* **2017**, *7* (2), 029901.

(54) Lee, Y. S.; Heo, J.; Siah, S. C.; Mailoa, J. P.; Brandt, R. E.; Kim, S. B.; Gordon, R. G.; Buonassisi, T. Ultrathin Amorphous Zinc-Tin-Oxide Buffer Layer for Enhancing Heterojunction Interface Quality in Metal-Oxide Solar Cells. *Energy Environ. Sci.* **2013**, *6* (7), 2112–2118.

(55) Chen, Z.; Dong, Q.; Liu, Y.; Bao, C.; Fang, Y.; Lin, Y.; Tang, S.; Wang, Q.; Xiao, X.; Bai, Y.; Deng, Y.; Huang, J. Thin Single Crystal Perovskite Solar Cells to Harvest Below-Bandgap Light Absorption. *Nat. Commun.* **2017**, *8* (1), 1–7.

(56) Li, C.; Hisatomi, T.; Watanabe, O.; Nakabayashi, M.; Shibata, N.; Domen, K.; Delaunay, J. J. Positive Onset Potential and Stability of Cu_2O-Based Photocathodes in Water Splitting by Atomic Layer Deposition of a Ga_2O_3 Buffer Layer. *Energy Environ. Sci.* **2015**, *8* (5), 1493–1500.

(57) Chua, D.; Kim, S. B.; Gordon, R. Enhancement of the Open Circuit Voltage of Cu_2O/Ga_2O_3 Heterojunction Solar Cells through the Mitigation of Interfacial Recombination. *AIP Adv.* **2019**, *9* (5), 055203.

(58) Zhu, L.; Shao, G.; Luo, J. K. Numerical Study of Metal Oxide Heterojunction Solar Cells. *Semicond. Sci. Technol.* **2011**, *26* (8), 085026.